湖南大学学报（自然科学版）
Journal of Hunan University (Natural Sciences)

第 50 卷 第 2 期
2023 年 2 月

Available online at http://jonuns.com/index.php/journal/index

Vol. 50 No. 2
February 2023

Open Access Article

https://doi.org/10.55463/issn.1674-2974.50.2.8

A Self-Balancing PSO-Tunned PI Controller for Integrating Parallel Converters with Variable Renewable Sources

Farhan Mumtaz*, Nor Zaihar Yahaya*

Department of Electrical and Electronics Engineering, Universiti Teknologi PETRONAS, Seri Iskandar, Malaysia

* Corresponding authors: farhan_19001785@utp.edu.my, norzaihar-yahaya@utp.edu.my

Received: December 16, 2022 ▪ Review: January 13, 2023 ▪ Accepted: February 7, 2023 ▪ Published: February 27, 2023

Abstract: This study aims to propose a system designed to fulfill the current and future energy requirements of commercial and domestic consumers. Recently, renewable energy generation methods obtained a higher priority in industrial applications to reduce and replace using hazardous fossil fuel-based energy generation methods. Conventional power generators generate AC voltage, which is incompatible with many modern appliances, requiring power conversion circuits. Power conversion circuits can make the overall system expensive and induce superfluous complexity in the system structure and control. In contrast, most renewable energy sources, such as photovoltaic and fuel cells, have inherent DC output voltage, and thus, the importance of DC systems inevitably surpasses the application of AC systems. In this framework, this paper focuses on the generation of multiple DC voltage levels. Three DC voltage levels were considered according to the IEC 60038 standard of the International Electrotechnical Commission. To generate multiple DC voltage levels, a parallel combination of power cells is used, where each power cell consists of a DC-DC converter. For adequate control, a particle swarm optimization tunned proportional integral (PSO-PI) controller applies. Three case studies evaluated the performance of the proposed system based on transient response and voltage ripples. For case study 1, the input and output conditions are kept constant; for case study 2, the input voltage is iterated, and the output load is kept constant; for case study 3, the input voltage is iterated, respectively the output load is also iterated with different load settings. In all case studies, the transient response is less than 0.15 s, and the voltage ripple is less than 5%.

Keywords: DC-DC converters, power cells, renewable energy, particle swarm optimization, controller.

用于集成具有可变可再生能源的并联转换器的自平衡粒子群优化算法调优 PI 控制器

摘要：本研究旨在提出一個旨在滿足商業和家庭消費者當前和未來能源需求的系統。最近，可再生能源發電方法在工業應用中獲得了更高的優先級，以減少和取代使用有害的基於化石燃料的能源發電方法。傳統的發電機產生交流電壓，這與許多現代電器不兼容，需要電源轉換電路。電源轉換電路會使整個系統變得昂貴，並導致系統結構和控製過於復雜。相比之下，大多數可再生能源，如光伏和燃料電池，都具有固有的直流輸出電壓，因此，直流系統的重要性不可避免地超過了交流系統的應用。在此框架下，本文重點研究了多個直流電壓電平的生成。根據國際電工委員會的國際電工委員會 60038 標準，考慮了三個直流電壓電平。為了產生多個直流電壓電平，使用並聯組合的電池，其中每個電池由一個直流-直流轉換器

組成。為了充分控制，應用了粒子群優化調諧比例積分控制器。三個案例研究根據瞬態響應和電壓紋波評估了所提出系統的性能。對於案例研究 1，輸入和輸出條件保持不變；對於案例研究 2，輸入電壓迭代，輸出負載保持不變；對於案例研究 3，輸入電壓被迭代，輸出負載也在不同的負載設置下被迭代。在所有案例研究中，瞬態響應均小於 0.15 秒，電壓紋波小於 5%。

关键词：直流-直流轉換器、電池、可再生能源、粒子群優化、控制器。

1. Introduction

The DC nano-grid (NG) idea offers a promising option for integrating renewable energy sources into the residential power system [1, 2]. Energy storage systems (ESS) must be in an islanded NG system to provide voltage support and ensure stable operation [3–5]. Distributed power systems are another application for several DC-DC converters connected in parallel. A parallel DC-DC converters-based structure is a specific system design where multiple DC-DC converters are connected in parallel with different voltages in a distributed residential NG system [6–8].

Currently, energy generation methods are evolving, and thus, using renewable energy sources is getting preferred globally compared to conventional energy generation methods [9–11]. Photovoltaic, fuel cell, and wind turbines are some of the frequently used renewable energy generation sources globally. The selection of RES is crucial, and site profiling is the best solution for this. Since all the RESs have their share of limitations. Thus, hybridizing multiple RES is a possible way to overcome this issue. Wind turbines are widely used in hybrid renewable energy systems (HRES), as wind energy is readily available throughout the day (Fig. 1).

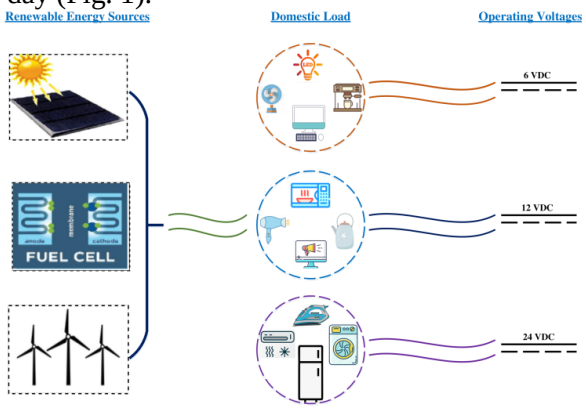

Fig. 1 Hybrid renewable energy sources HRES and consumer power requirements [10, 12]

Other wind turbines have high power generation capability with easy output power conversion to DC voltage that can be consumed directly and stored. Overall, RES has numerous advantages, besides being environment friendly; it has many times an inherent DC output voltage. Thus, the DC voltage is compatible with most domestic and commercial appliances. Modern home appliances are generally categorized into different segments per their application, as shown in Fig. 1. Small-scale appliances require a low-level DC voltage level, and similarly, medium and high-scale appliances require different DC voltage levels [12]. IEC 60038 of the International Electrotechnical Commission standardized these DC voltage levels [13].

A DC-DC converter is a vital component of DC nano-grids [14]. Nano-grids can use photovoltaic, fuel cells, wind turbines, and other RESs. Wind turbines require rectifiers to convert the AC voltage into DC voltage to enhance the efficiency of nano-grids, whereas photovoltaic and fuel cells generate DC voltage. Furthermore, DC-DC converters ensure that the output voltage remains constant irrespective of the changing input and output conditions [15, 16]. Numerous DC-DC converter topologies are available.

Conventional converter topologies include the buck converter, which steps down the supplied input voltage as per the reference voltage value [17]. The boost converter steps up the supplied voltage considering the reference voltage value [18]. Buck-boost converter topology is the combination of buck and boosts converter in a single converter topology [19]. Buck-boost converter topology performs voltage step-down, voltage step-up, or keeps the voltage constant by comparing it with the reference voltage. Furthermore, recent converter topologies are the advanced versions of the aforementioned conventional converter topologies.

The overall performance of the DC-DC converter is contingent on the applied control technique [16]. Steady-state and transient-state responses are the main parameters for selecting the control technique.

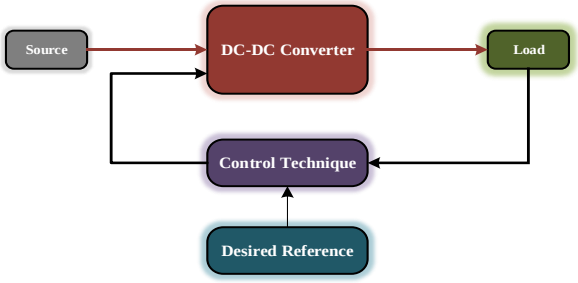

Fig. 2 Operation of the DC-DC converter

Fig. 2 depicts the integration of the feedback control loop with the DC-DC converter. For the optimum operation of the DC-DC converter, the feedback from the load side is compared with the desired reference voltage to avoid abnormality at the load side. To ensure a constant output voltage level, the DC-DC converter requires an appropriate switching duty cycle achieved by the optimum performance of the control technique [20, 21].

Fuzzy logic control (FLC) is a robust non-linear control. Its operation mimics the human mind and makes decisions based on the assigned condition known as a rule base. FLC performs the linguistic information-based fuzzy logic process of assigning outputs. The knowledge base and the inference engine make up the controller. The membership functions and fuzzy rules that comprise the knowledge base are derived from knowledge about the system's operation with the environment [22–24].

Slide mode control (SMC) is another robust control technique. The sliding mode control strategy directs the system state variables toward a specified surface known as the sliding surface and maintains the state variables' trajectory on this surface. Asymptotic convergence of the state variables to zero can be achieved after they reach the sliding surface. The SMC control scheme struggles with conceptual/implementation complexity compared to conventional linear controllers, which already provide adequate control properties in DC-DC control applications [19, 25].

Model predictive control (MPC) is a control technique that predicts future values for the system. It is an advanced version of SMC control and has better efficiency than SMC [26, 27].

For decades, the proportional-integral (PI) control technique is opted for industrial applications. PI works on the received error transmitted to the controller and makes it possible to calculate k_p and k_i values. The k_p and k_i gains are coupled with the error signal that goes to the PI controller [14, 28, and 29]. Additionally, the PI controller can easily be integrated with other control and optimization techniques Fig. 3.

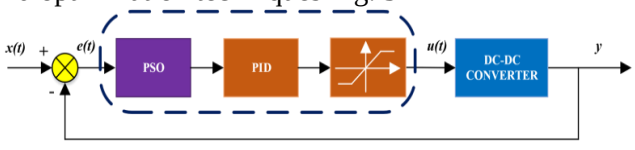

Fig. 3 PSO-tunned PI control integration with DC-DC converter

In this framework, the main contributions of the proposed work are as follows:

- To design energy generation architecture considering the future energy trends of multi-level DC voltage that will eliminate the additional power conversion circuitry to enhance the efficiency of renewable energy power generation systems.
- To achieve the balanced output of power cells, the integration of an adequate PSO-tuned PI control algorithm that effectually replaces the use of conventional control techniques and thus overcomes their limitations.
- The self-balanced architecture of power cells is used to reduce the operational deficiencies of multi-level converter architectures while improving the power quality and maintaining nominal component stress on the power converters.
- Furthermore, the performance evaluation of the control algorithm, transient state response, and voltage ripple in all case studies are critically analyzed.

2. Configuration of the Single Unit DC-DC Converter

The equivalent circuit of the DC-DC converter depicted in Fig. 4 includes two inductors (L_1 and L_2) and two capacitors; the first capacitor C_1 (acts as an isolation barrier between the input and output section), whereas C_2 is the output capacitor, diode D_1 that is used as a passive switch and the active power switch is S. The power switch is operated using the switching frequency f_s having a duty ratio D.

2.1. Operation of a Single Unit DC-DC Converter

This section comprises of operational modes for a single unit of a converter in the continuous conduction mode (CCM).

2.1.1. Mode I

In this mode, the active power switch S, is turned ON for the time interval [t_0, t_1]. The input source V_{in} charges the inductor L_1. As the switch S is ON, the switch path represents a short path. Therefore, the voltage across the inductor L_1 is equal to the input source V_{in}, and the voltage across the inductor L_2 is equal to the capacitor voltage V_{C1}. Consequently, the passive switch diode D_1 is not active; hence acts as an open circuit, and the capacitor delivers the energy to the inductor L_2.

The following expressions are derived by applying KVL and KCL on the converter's equivalent circuit shown in Fig. 5.

$$V_{L1} = V_{in} \quad (1)$$

$$V_{L2} = V_{C1} \quad (2)$$

$$V_{L2} = V_s \quad (3)$$

$$I_{C1} = -I_0 \quad (4)$$

$$I_{C1} = -\frac{V_0}{R} \quad (5)$$

$$\{V_{L1} = V_{in}, \quad 0 \le T_S \le DT_S \quad (6)$$

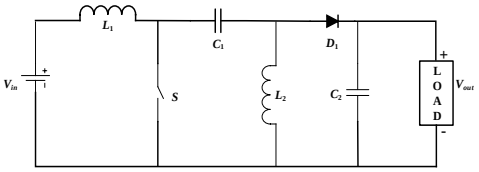

Fig. 4 Equivalent circuit of the DC-DC converter

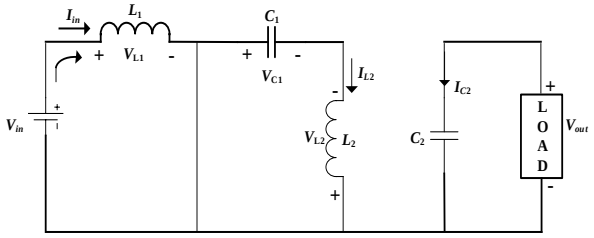

Fig. 5 Equivalent circuit of the DC-DC converter in Mode I

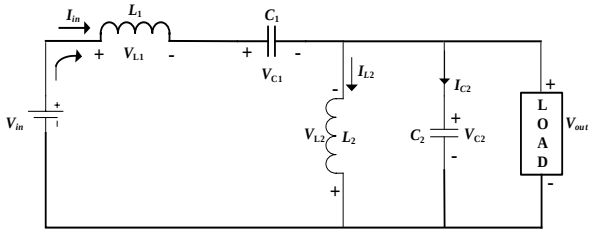

Fig. 6 Equivalent circuit of the DC-DC converter in Mode II

2.1.2. Mode II

In this mode, the active power switch *S* is turned OFF for the time interval [t_1, t_2]. During this mode, the inductors L_1 and L_2 supply energy to the load. Furthermore, capacitors C_1 & C_2 are also being charged by the inductors L_1 & L_2.

By applying KVL and KCL on the equivalent circuit of the converter, as depicted in Fig. 6 the following expressions are attained.

$$V_{L1} = V_{in} - V_{C1} - V_O \quad (7)$$

$$V_{L2} = -V_O \quad (8)$$

$$I_C = I_D - I_O \quad (9)$$

$$I_C = I_D - \frac{V_O}{R} \quad (10)$$

$$\{V_{L1} = -V_O, \qquad DT_S \le T_S \le T_S \quad (11)$$

By applying volt-second balance on (6) and (11), we get (12).

$$\int_0^{DTs} V_L{}^I dt + \int_0^{(1-D)Ts} V_L{}^{II} dt = 0 \quad (12)$$

where the superscripts I and II represent the operation modes of the converter. By solving equation (12), the voltage gain is attained as (13).

$$\frac{V_O}{V_{in}} = \frac{D}{1-D} \quad (13)$$

2.2. Component Selection

The design of the DC-DC converter comprises the appropriate values of capacitors, inductors, and load resistance, as depicted in Table 1.

Table 1 Parameter specification for the DC-DC converter

Parameters	**Symbol**	**Values**
Input Voltage	V_{in}	10 V -20 V
Output voltage of the converter 1	V_{out1}	6 V
Output voltage of the converter 2	V_{out2}	12 V
Output voltage of the converter 3	V_{out3}	21 V
Input inductor	L_1	0.325 mH
Output inductor	L_2	0.325 mH
Input capacitor	C_1	0.0726 mF
Output capacitor	C_2	0.102 mF

2.2.1. Inductor Selection

To obtain a suitable value of inductors, mathematical representation is expressed in (16).

$$\Delta I_L = \frac{V_{in}}{L} * DT_s \quad (14)$$

$$\Delta I_L = \frac{V_{in}}{f_s L} * D \quad (15)$$

$$L_1 = L_2 = \frac{V_{in}}{\Delta I_L * f_s} * D \quad (16)$$

2.2.2. Capacitor Selection

To find the appropriate value of coupling capacitor C_1, a mathematical expression is derived in (19).

$$\Delta V_{C1} = \frac{I_{out}}{C} * DT_s \quad (17)$$

$$\Delta V_{C1} = \frac{I_{out}}{f_s C} * DT_s \quad (18)$$

$$C_1 = \frac{V_{out}}{R f_s \Delta V_{C1}} * D \quad (19)$$

To obtain the optimum value for the output capacitor *C*, (20) is used.

$$C_2 = \frac{I_{out}}{\Delta V_C * 0.5 * f_{sw}} * D \quad (20)$$

$$R = \frac{V_{out}}{I_{out}} \quad (21)$$

$$\Delta I_L = I_{in} * 40\% \quad (22)$$

$$I_{out} = \frac{V_{out}}{V_{in}} * 40\% \quad (23)$$

Modeling of the converter topology also includes the calculation of output load as expressed in (21), and the output current is depicted in (22) and (23).

The duty cycle ratio expressed in (24), for the optimum operation of the DC-DC converter.

$$D = \frac{V_{out} + V_D}{V_{in} + V_{out} + V_D} \quad (24)$$

3. Implementation Process of the Proposed System

The proposed parallel combination of the DC-DC converters is integrated with RES. The red dotted line is focused on the proposed system, as shown in Fig. 7. The internal structural design of cell 1 is clearly shown in Fig. 8. However, the representation of power cell 2 and power 3 uses subsystem blocks. The proposed system is tested with variable load conditions, including the resistive load and a combination of loads,

as depicted in Fig. 9.

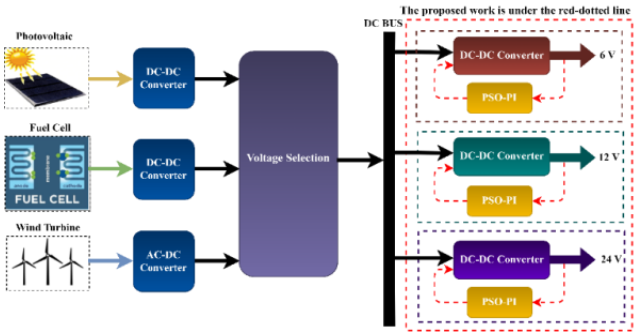

Fig. 7 Block diagram of self-balancing converters integrated with renewable energy sources

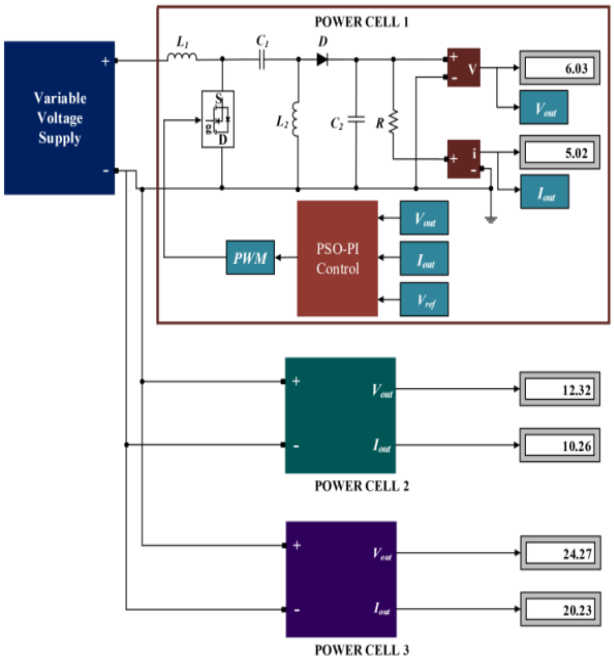

Fig. 8 Simulation model of the proposed system using MATLAB Simulink

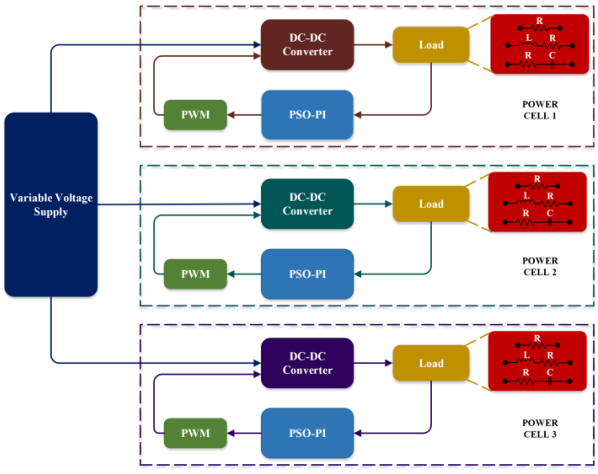

Fig. 9 PSO-tunned PI control integration with a DC-DC converter and different loads

3.1. Particle Swarm Optimization-Tunned Proportional Integral Controller

The particle swarm optimization (PSO) technique is based on social behavior ideologies. PSO includes a population of particles, where each particle in the population signifies a possible solution. Each particle possesses a significant velocity, which is iterated with an updated equation based on the collective and individual experience of particles [31]. The aim is to achieve the best solution by changing the position of each particle by a specified velocity, as depicted in Fig. 10.

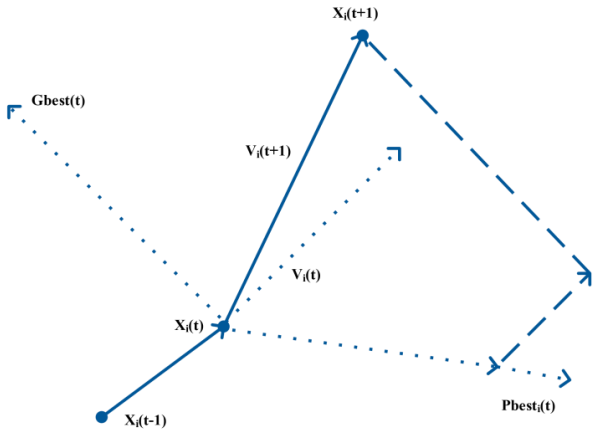

Fig. 10 Visual illustration of the PSO

Initially, the particles are scattered or equally distributed in the search space. Later, particles are assessed using a cost function, and the rest of the particles update theirs following the path of the particle having the best solution with an adequate velocity. The velocity depends on three parameters, as elaborated in (25): previous iteration velocity, particle best solution (P_{besti}), and global best solution (G_{best}) [32, 33].

$$V_i(t+1) = WV_i(t) + CR_1 \otimes (P_{besti} + G_{best} - 2X_i(t)) \quad (25)$$

where W denotes the weight; C denotes the acceleration factor; R_1 is a vector having mixed values uniformly distributed from 0 to 1; P_{besti} represents the cost function values of the personal best position of particle i; G_{best} denotes the cost function values of the global best particle at a particular moment.

Furthermore, to ensure a prompt feedback response, the proportional-integral (PI) control is tunned using the PSO technique in the proposed system. The calculation for the suitable gains of the PI control expression is depicted in (26).

$$u(t) = k_p e(t) + k_i \int_0^t e(\tau) d\tau \quad (26)$$

where k_p represents the proportional gain value; k_i represents the integral gain value of the PI control. The input voltage level feedback response determines the duty cycle ratio of the parallel converters, as shown in Table 2.

Table 2 Calculated duty cycle ratio's for all cells

Varying input voltage	Power cell 1 (6 V) duty cycle ratio *D*	Power cell 2 (12 V) duty cycle ratio *D*	Power cell 3 (24 V) duty cycle ratio *D*
10 V	39.3%	55.5%	71%
15 V	30.2%	45.4%	62%
20 V	24.5%	38.4%	55%
17 V	27.6%	42.3%	59%
14 V	31.7%	47.1%	63.6%

4. Performance Analysis and Simulation Results

To evaluate the DC converter's performance, all significant parameters are depicted in Table 3. All the parameter values are observed at the peak conditions, as shown in Fig. 11.

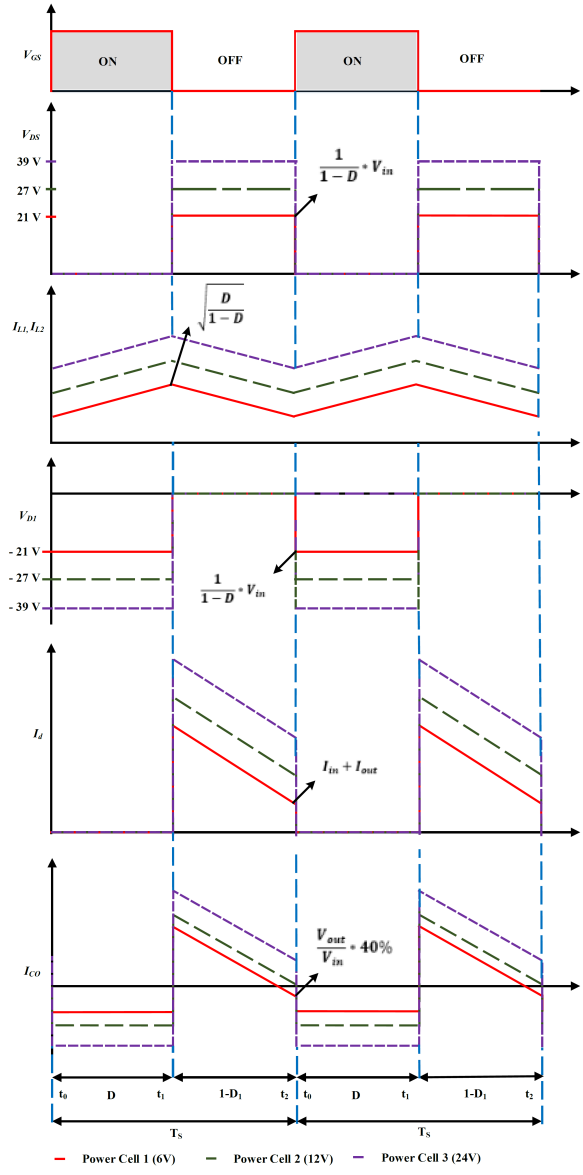

4.1. Case Study 1

In case study 1, the proposed system is simulated with constant input voltage with the output response depicted in Table 4. The output response of the proposed system has been stabilized without any abnormal transients, as shown in Fig. 12.

The voltage ripple is also observed for all three power cells: it is 1.66% for power cell 1, for power cell 2, the voltage ripple is 1.83%, and for power cell 3, the voltage ripple is 2.5%. Thus, all power cells have a voltage ripple of less than 5% per the allowable limits [34]. Moreover, all three power cells achieved their desired output voltages V_{out} at 0.22 s, as illustrated in Fig. 12, whereas the output currents for all power cells were also stabilized at 0.22 s, as depicted in Fig. 13.

4.2. Case Study 2

In case study 2, the proposed system is simulated under varying input voltage at different time intervals.

For power cell 1, during the transition at 0.2 s, 0.4 s, 0.6 s, and 0.8 s, the transient response was 0.12 s with an overshoot voltage of 10.4 V, 0.11 s with an overshoot voltage of 9.4 V, 0.14 s with an undershoot voltage of 5.3 V, and 0.13 s with an undershoot voltage of 4.8 V, as shown in Fig. 14 (a).

For power cell 2, during the transition at 0.2 s, 0.4 s, 0.6 s, and 0.8 s, the transient response at 0.1 s with an overshoot voltage of 22 V, 0.1 s with an overshoot voltage of 19.4 V, 0.12 s with an undershoot voltage of 10.2 V, and at 0.12 s with an undershoot voltage of 9.2 V as depicted in Fig. 15 (a).

For power cell 3, during the transition at 0.2 s, 0.4 s, 0.6 s, and 0.8 s, the transient response was 0.1 s with an overshoot voltage of 42 V, at 0.1 s with an overshoot voltage of 37 V, at 0.07 s with an undershoot voltage of 19.6 V, and 0.085 s with an undershoot voltage of 16.6 V as shown in Fig. 15 (a). V

Voltage ripple is also analyzed after each voltage transition: for power cell 1, at 0.35 s, the voltage ripple is 2.33%, at 0.5 s - 2.16%, at 0.75 s - 2.66%, at 0.95 s - 3.83% (Fig. 14 (b)), for power cell 2, at 0.35 s the voltage ripple is 3.33%, at 0.56 s - 1.66%, at 0.75 s - 1.66%, at 0.955 s -2.08% (Fig. 15 (b)), and for power cell 3, at 0.355 s, 0.555 s, 0.755 s, and at 0.955 s the voltage ripple is same 2.5 V, as illustrated in Fig. 16 (b). The voltage ripple observed is within the standards [34] and is less than 5% for all three power cells in this case study. The output current for all three converters has satisfactory results under varying input voltage transitions, as depicted in Fig. 17.

4.3. Case Study 3

In case study 3, the proposed system is simulated with variable input voltage and variable load conditions (Table 4).

For power cell 1, during the transitions at 0.3 s, 0.5 s, and 0.7 s, the transient response at 0.1 s with an undershoot voltage of 5.2 V, at 0.12 s with an overshoot voltage of 10.9 V, and 0.12 s with an undershoot

voltage of 5.3 V and overshoot voltage of 6.5V depicted in Fig. 18 (a).

For power cell 2, during the transitions at 0.3 s, 0.5 s, and 0.7 s, the transient response at 0.13 s with an overshoot voltage of 12.25 V and an undershoot of 10.2 V, at 0.12 s with an overshoot voltage of 20 V, and, at 0.02 s with an overshoot of 13.45 V and an undershoot voltage of 10 V as shown in Fig. 19 (a).

For power cell 3, during the transitions at 0.3 s, 0.5 s, and 0.7 s, the transient response at 0.06 s with an overshoot voltage of 24.5 V and undershoot of 18 V, at 0.1 s with an overshoot voltage of 35 V, and, at 0.03 s with an over-shoot voltage of 26.5 V and an undershoot of 18.5 V as illustrated in Fig. 20 (a).

Voltage ripples are also analyzed after each voltage transition; for power cell 1, at 0.406 s, the voltage ripple is 4 %; at 0.695 s, the voltage ripple is 4.5 %; and at 0.725 s, the voltage ripple is 4.16 %, as shown in Fig. 18 (b), for power cell 2, the voltage ripple was observed at 0.406 s the voltage ripple is 4 %, at 0.695 s the voltage ripple is 4.58 %, and for 0.725 s the voltage ripple is 4.58 %, as shown in Fig. 19 (b) for power cell 3, after the voltage ripple was observed at 0.406 s the voltage ripple is 4.58 %, at 0.695 s the voltage ripple is 4.9 %, and at 0.725 s the voltage ripple is 4.9 %, as shown in Fig. 20 (b) The voltage ripple is observed within the standards [34] that is less than 5 % for all the three power cells in this case study. Fig. 21 shows the output current response.

5. Comparative Performance Analysis

The optimum performance of the proposed system gains by integrating it with an adequate control technique, as illustrated in Table 5. In [35] sliding mode control (SMC) technique combines with the converter topology. SMC has a quick tracking performance under moderately varying conditions. However, during the abrupt variation, SMC encounters an issue of chattering effect that results in large overshoots.

[36] presents state space modeling (SSM) control. It has a quick transient response and fewer overshoots, as discussed in [36]. However, the SSM control technique has a large drawback that requires in-depth system detailing. [30] depicts another robust and non-linear control technique, where the model predictive control (MPC) technique has a faster tracking response than SMC and has no chattering issues. However, MPC also persists with high computational time and complex algorithm structure.

In [37], fuzzy logic control (FLC) integrates with DC-DC converter topology. FLC possesses fewer overshoots and has a satisfactory reference tracking performance. Besides, these advantages also have drawbacks, such as high computational time and complex algorithm structure.

[38] presents the proportional-integral (PI) control technique; it has a simple structure and satisfactory performance. However, PI has a high steady state and transient response. Considering the abovementioned issues in PI control, the proposed system uses a hybridized one. Particle swarm optimization (PSO) is integrated with the PI control to acquire optimum results. The PI control gains iterate using the PSO, significantly improving the results.

The proposed system has a fast transient and steady-state response under varying operating conditions. Furthermore, the converter performance parameters, which include voltage gain, voltage ripple, and component stress, are under the allowable limits.

Table 3 DC-DC converter performance in all case studies

Parameters (Peak values)		**Switching stress (V_{DS})**	**Inductor current (I_L)**	**Diode voltage (V_{D1})**	**Diode current (I_d)**	**Capacitor current (I_{CO})**
Case Study 1	Converter 1 (6V)	21 V	0.6 A	-21 V	1.3 A	0.8 A
	Converter 2 (12 V)	27 V	1.3 A	-27 V	2.7 A	1.6 A
	Converter 3 (24 V)	39 V	4 A	-39 V	6.5 A	4.5 A
Case Study 2	Converter 1 (6V)	26 V	0.8 A	-26 V	1 A	1.5 A
	Converter 2 (12 V)	40 V	5.2 A	-40 V	6.5 A	5.2 A
	Converter 3 (24 V)	56 V	9 A	-56 V	13 A	12 A
Case Study 3	Converter 1 (6V)	21 V	22 A	-21 V	6.2 A	4 A
	Converter 2 (12 V)	30 V	8.2 A	-30 V	14.2 A	10 A
	Converter 3 (24 V)	45 V	17 A	-45 V	25 A	29 A

Table 4 Simulation results under different case studies

Case Studies																				
	Case study 1 (Fixed)		**Case study 2 (Variable voltage and fixed load)**										**Case study 3 (Variable voltage and variable load)**							
Time Intervals (s)	0 < t < 1 V_{in} = 15 V, R = 12 Ω		0 < t < 0.2 V_{in} = 10 V, R = 12 Ω		0.2 < t < 0.4 V_{in} = 15 V, R = 12 Ω		0.4 < t < 0.6 V_{in} = 20 V, R = 12 Ω		0.6 < t < 0.8 V_{in} = 17 V, R = 12 Ω		0.8 < t < 1 V_{in} = 14 V, R = 12 Ω		0 < t < 0.3 V_{in} = 10 V, R = 12 Ω		0.3 < t < 0.5 V_{in} = 10 V, R = 12 Ω L = 5 mH		0.5 < t < 0.7 V_{in} = 15 V, R = 8 Ω L = 1 mH		0.7 < t < 1 V_{in} = 15 V, R = 10 Ω C = 1000 µF	
	Output voltage and current of the converters under different case studies																			
	V_{out}	I_{out}	V_{out}	I_{out}	V_{out}	I_{out}	V_{out}	I_{out}	V_{out}	I_{out}	V_{out}	I_{out}	V_{out}	I_{out}	V_{out}	I_{out}	V_{out}	I_{out}	V_{out}	I_{out}
Converter 1	6.08 V	0.5 A	6.1 V	0.6 A	6.4 V	0.4 A	6.5 V	0.4 A	6.1 V	0.6 A	5.9 V	0.5 A	6.08 V	0.5 A	6.2 V	0.4 A	5.9 V	0.6 A	6.2 V	0.5 A
Converter 2	12.2 V	1 A	12.3 V	1.2 A	12.1	1.1 A	12.4 V	1.3 A	12.3 V	1.2 A	11.8 V	1.2 A	12.2 V	1 A	12.1 V	0.9 A	11.9 V	1.2 A	12.1 V	1.2 A
Converter 3	24.3 V	2 A	24.2 V	2.4 A	24.3	2.2 A	24.1 V	2.1 A	24.1 V	2.1 A	23.9 V	2.2 A	24.3 V	2 A	24.1 V	1.8 A	23.8 V	2.1 A	24.3 V	2.2 A

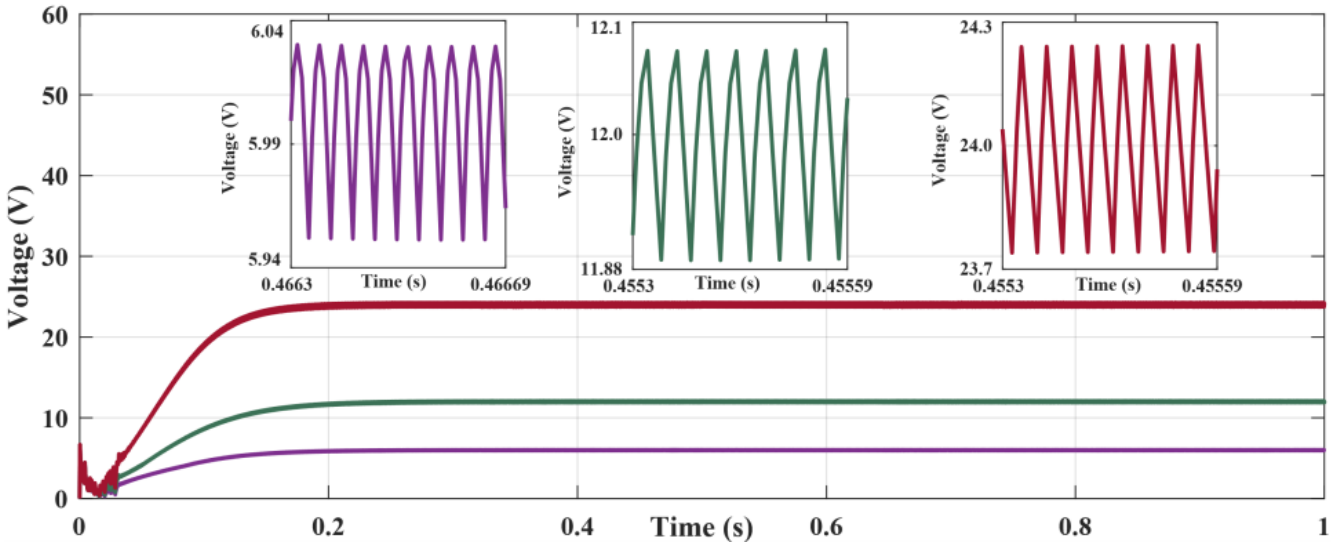

Fig. 12 Simulation results in Case Study 1: voltage ripples for all power cells

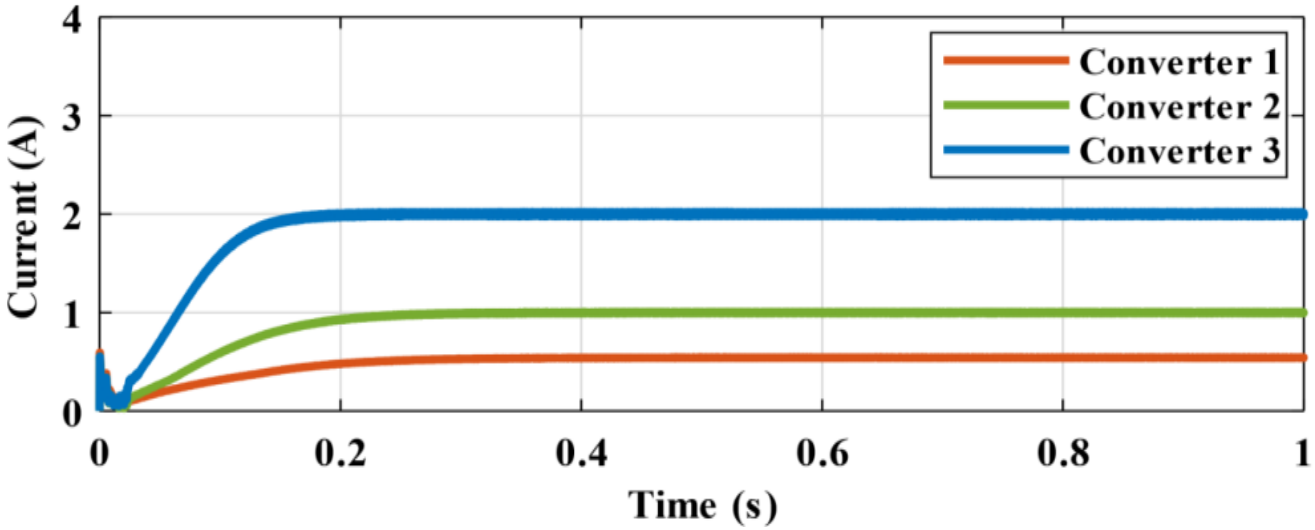

Fig. 13 Simulation results in Case Study 1: output current response for all power cells

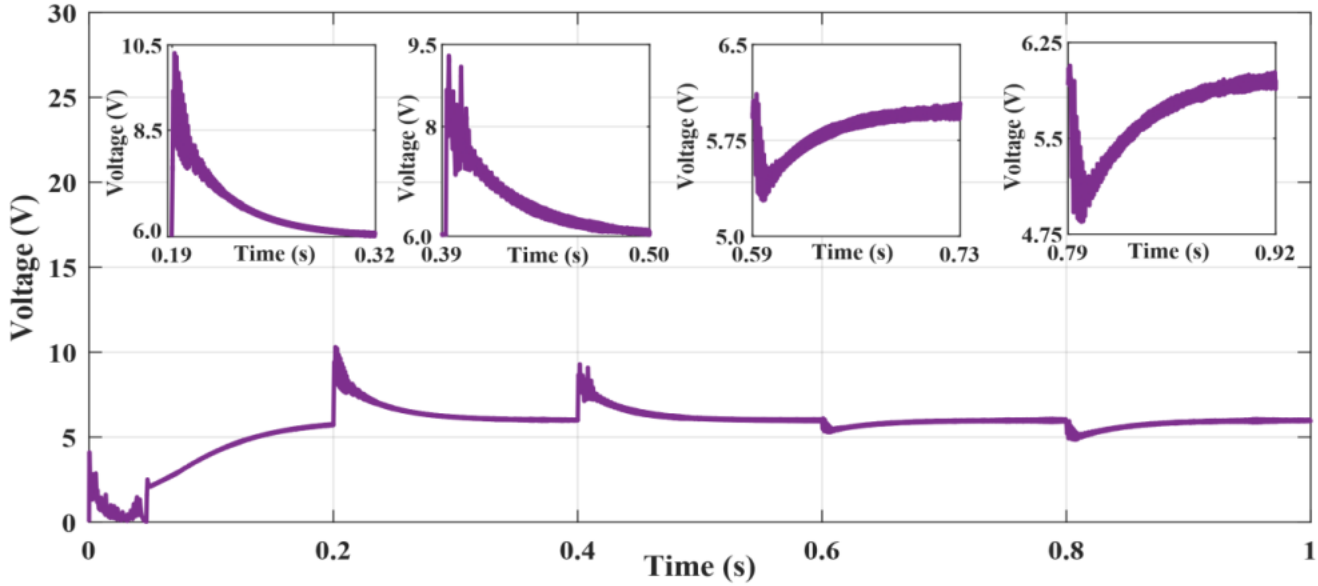

Fig. 14 (a) Simulation results in Case Study 2: transient response for power cell 1

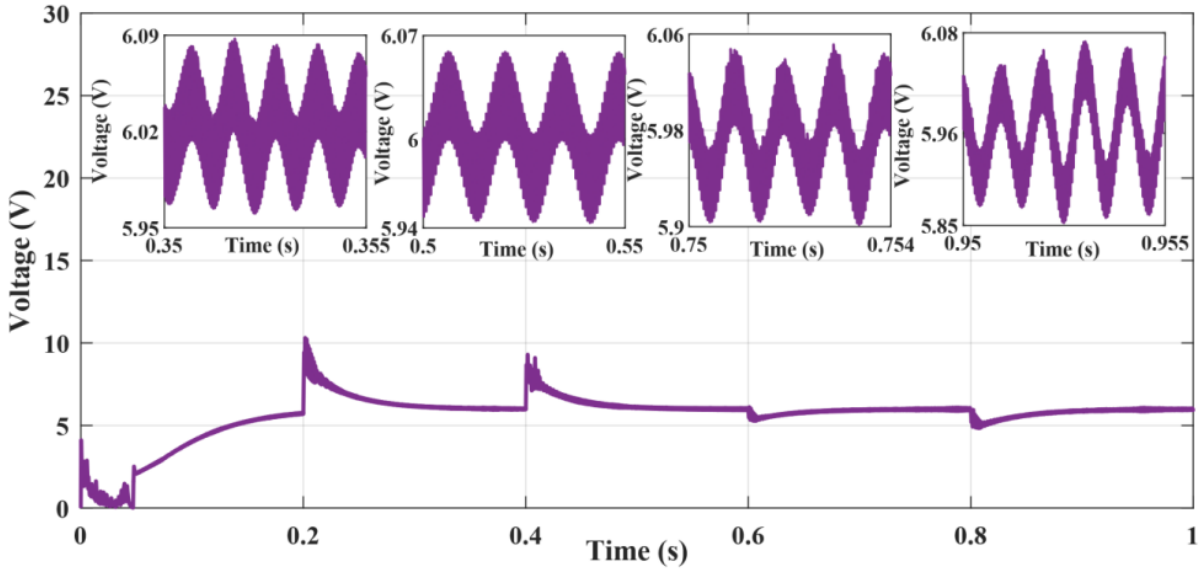

Fig. 14 (b) Simulation results in Case Study 2: voltage ripple response for power cell 1

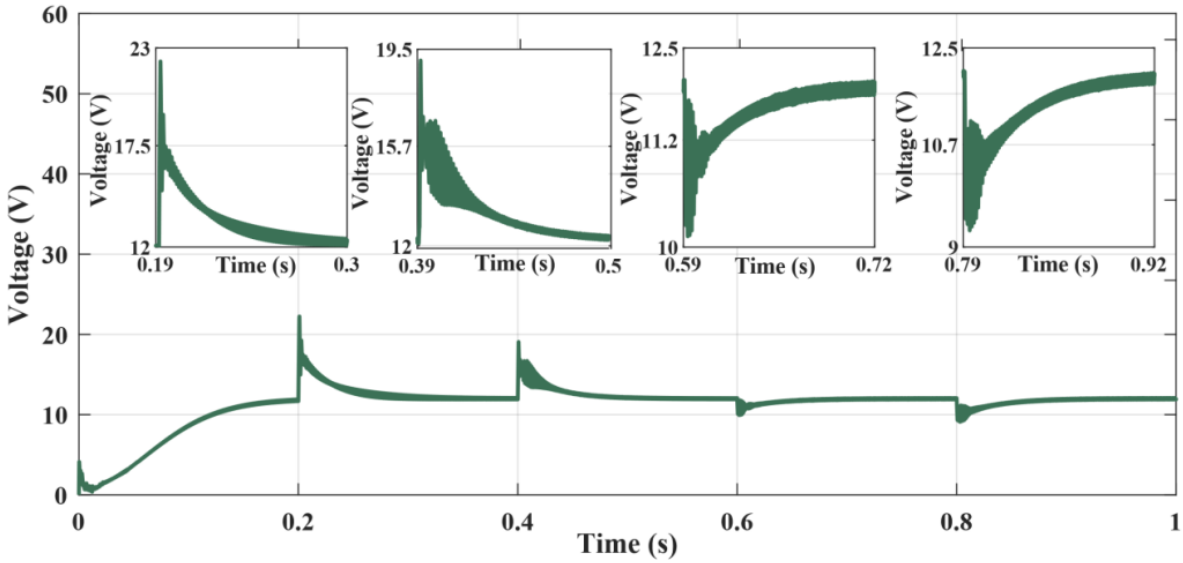

Fig. 15 (a) Simulation results in Case Study 2: transient response for power cell 2

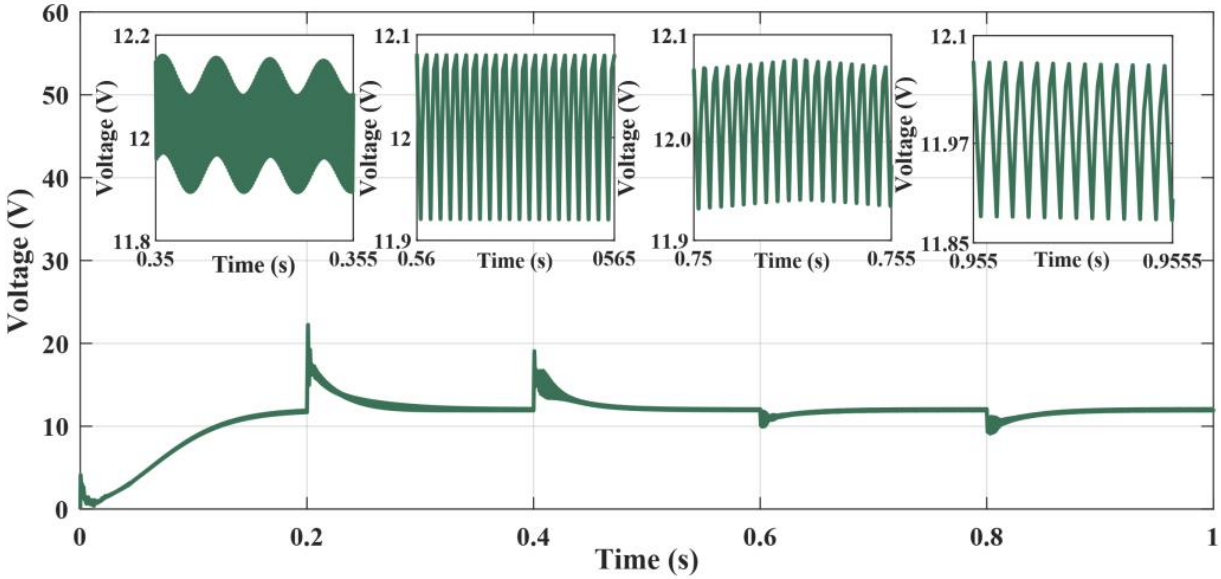

Fig. 15 (b) Simulation results in Case Study 2: voltage ripple response for power cell 2

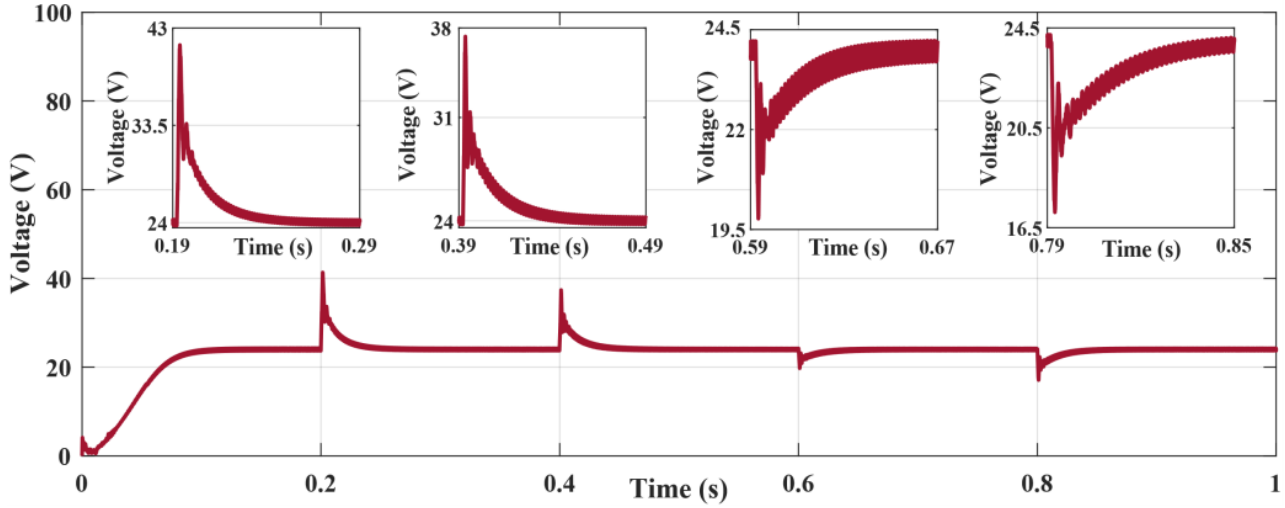

Fig. 16 (a) Simulation results in Case Study 2: transient response for power cell 3

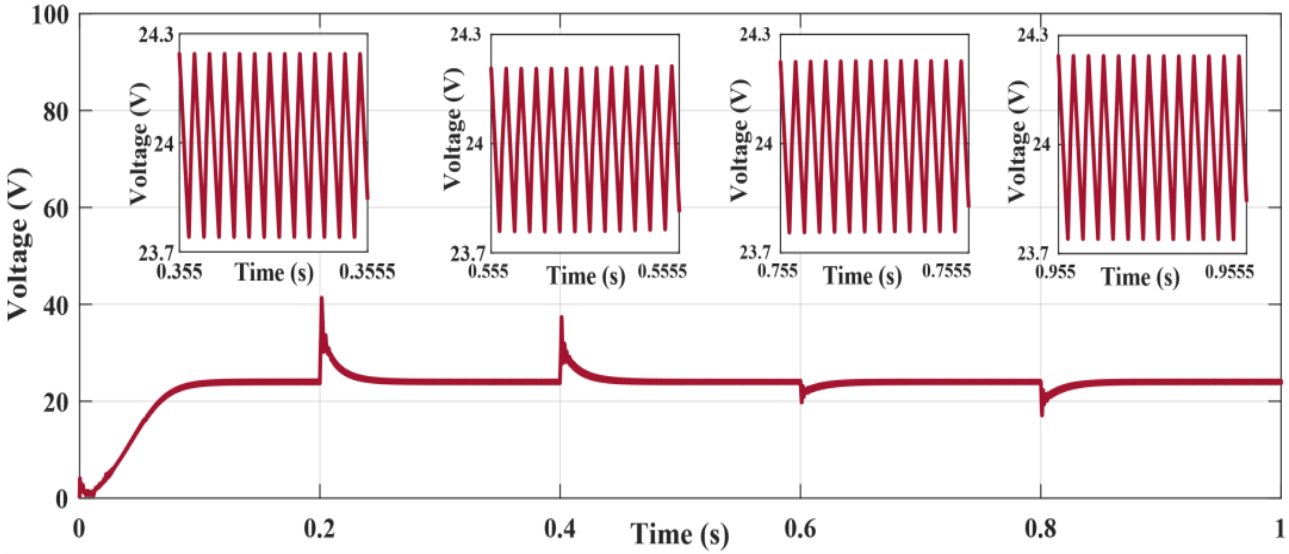

Fig. 16 (b) Simulation results in Case Study 2: voltage ripple response for power cell 3

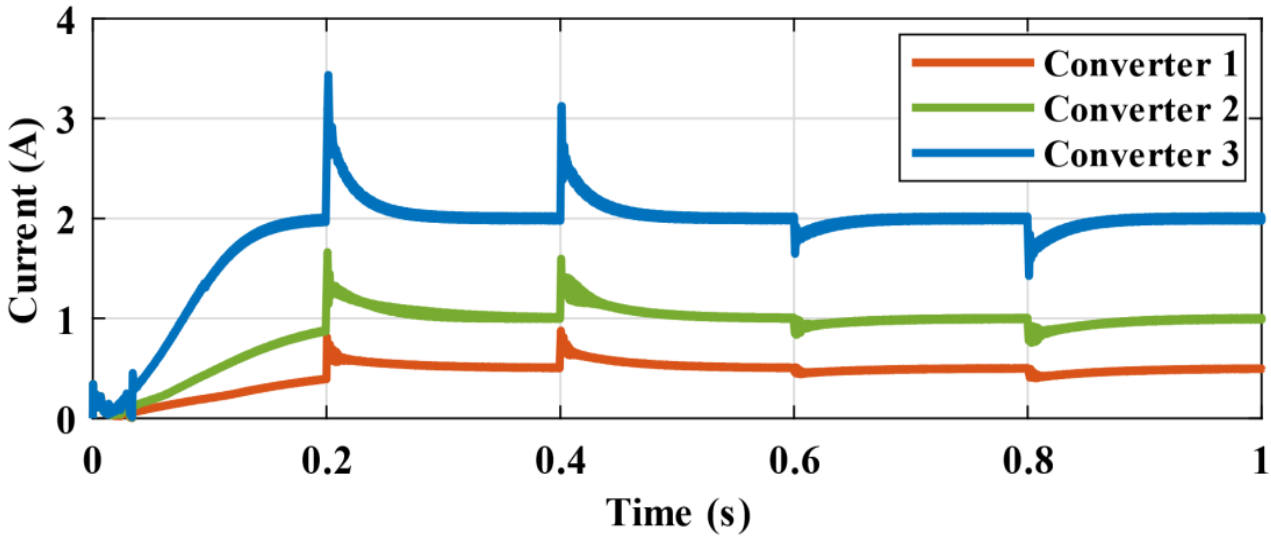

Fig. 17 Simulation results in Case Study 2: output current response for all power cells

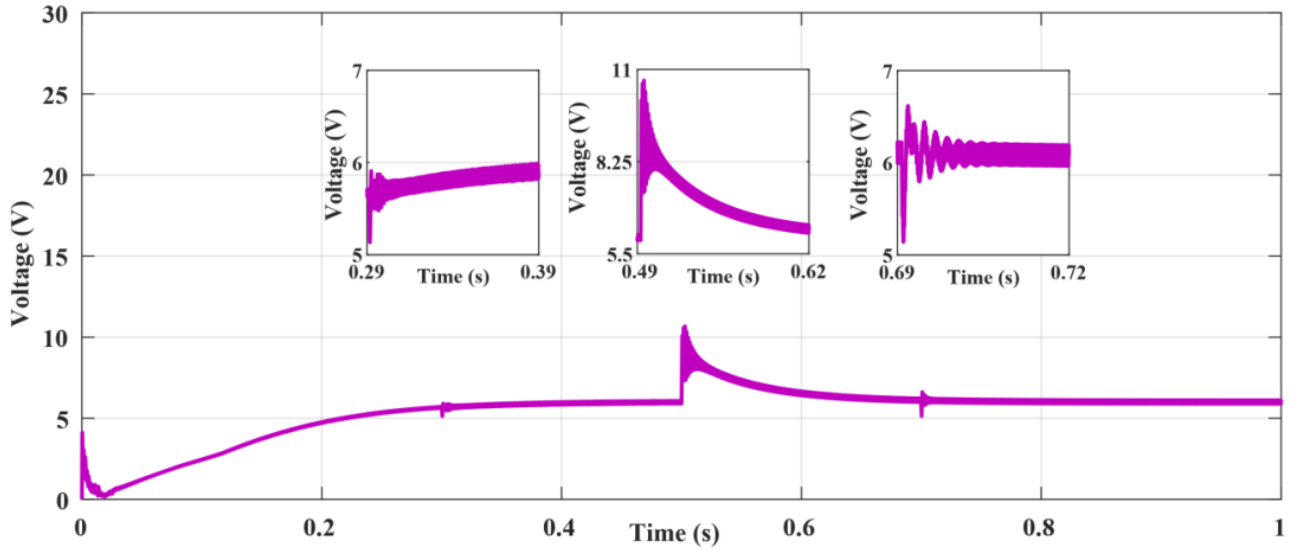

Fig. 18 (a) Simulation results in Case Study 3: transient response for power cell 1

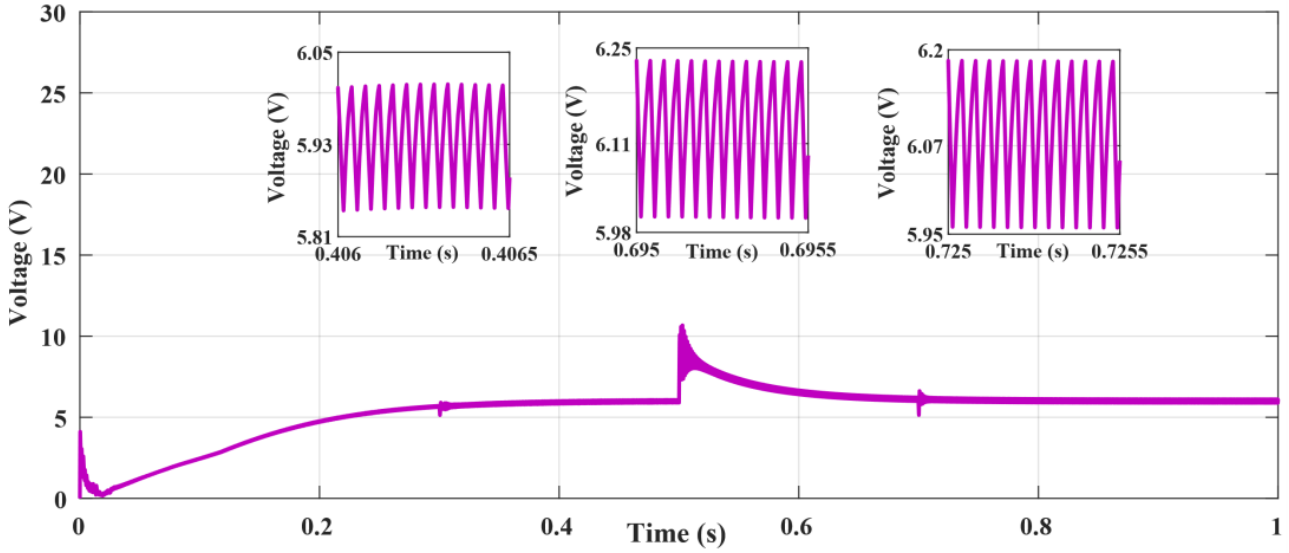

Fig. 18 (b) Simulation results in Case Study 3: voltage ripple response for power cell 1

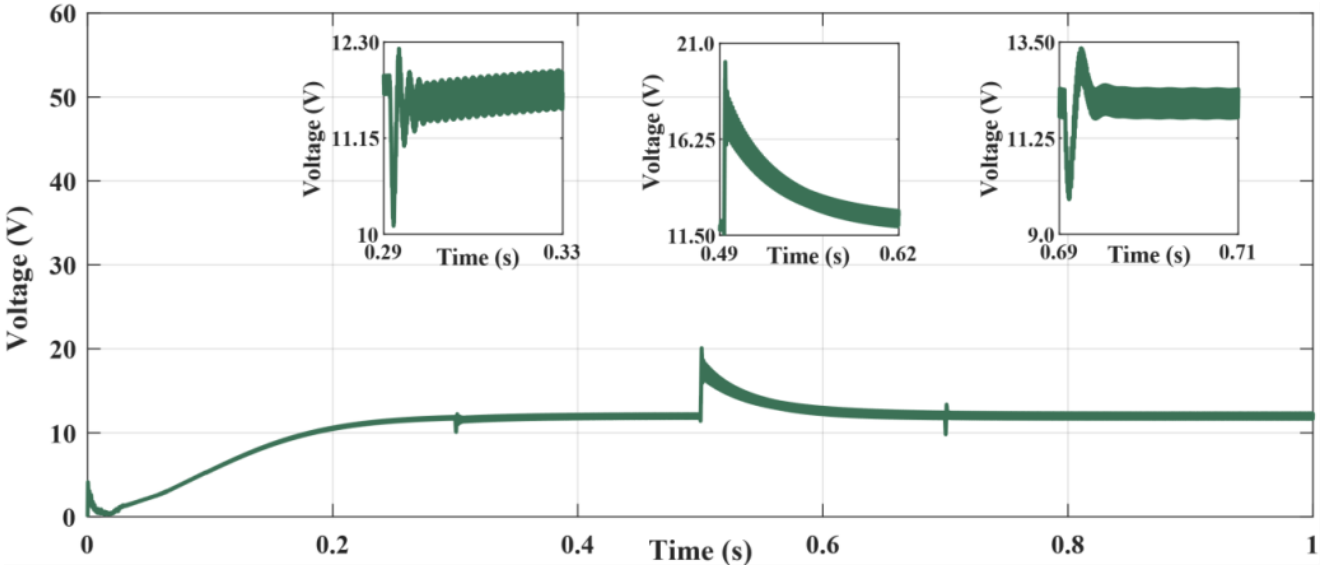

Fig. 19 (a) Simulation results in Case Study 3: transient response for power cell 2

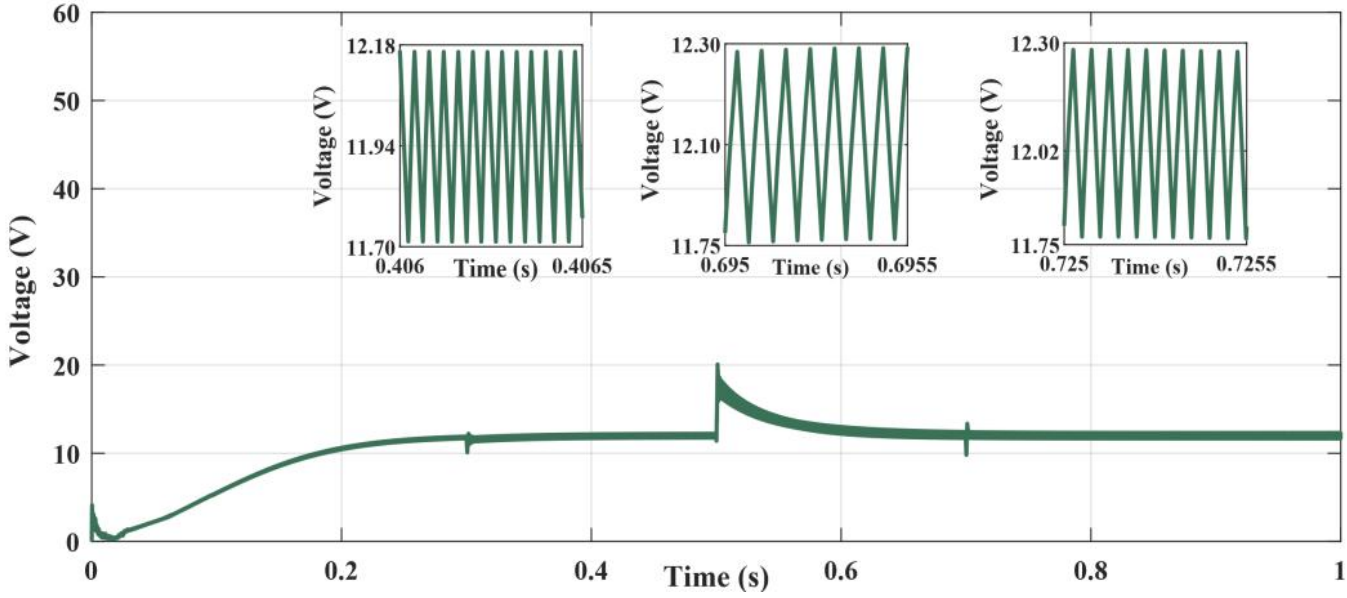

Fig. 19 (b) Simulation results in Case Study 3: voltage ripple response for power cell 2

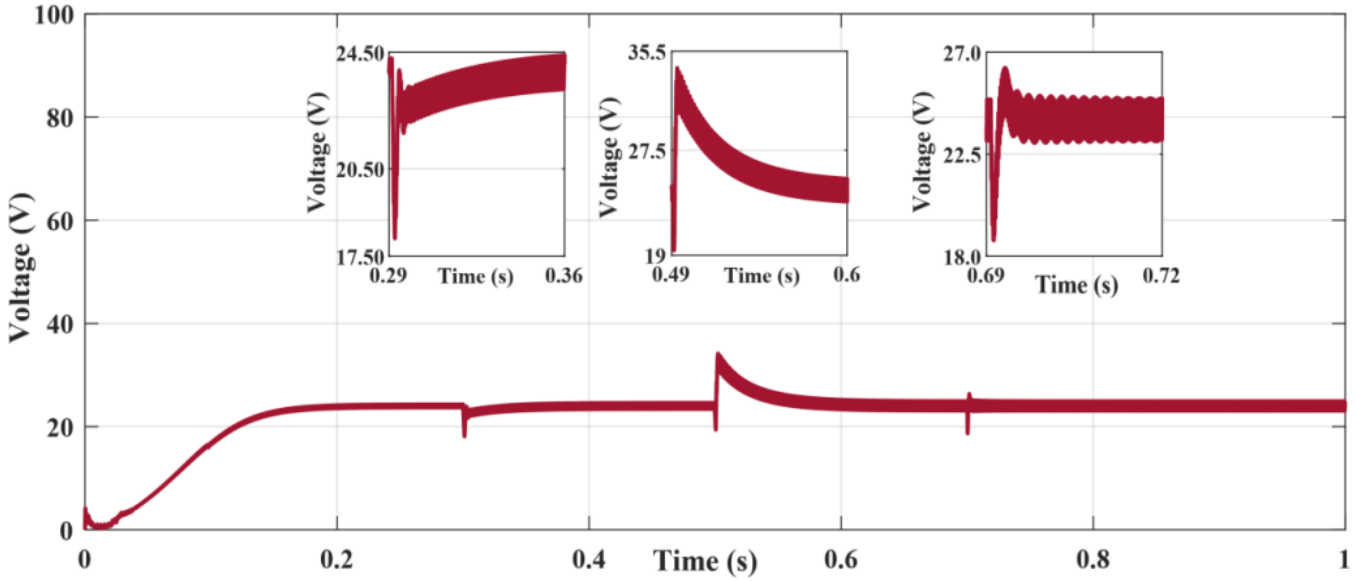

Fig. 20 (a) Simulation results in Case Study 3: transient response for power cell 3

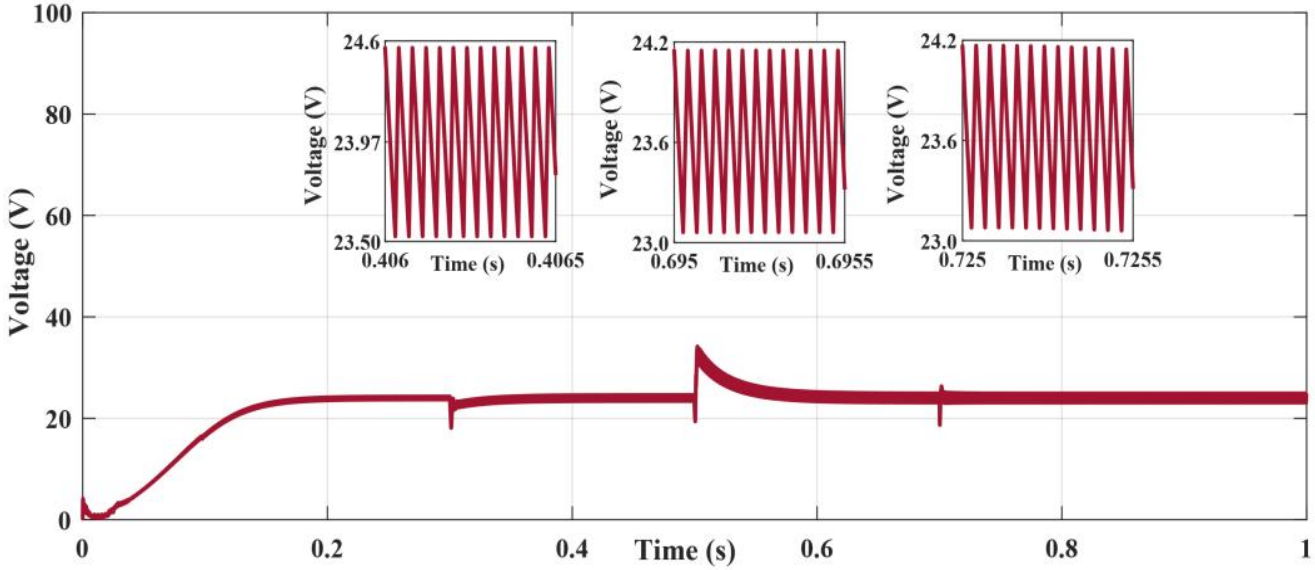

Fig. 20 (b) Simulation results in Case Study 3: voltage ripple response for power cell 3

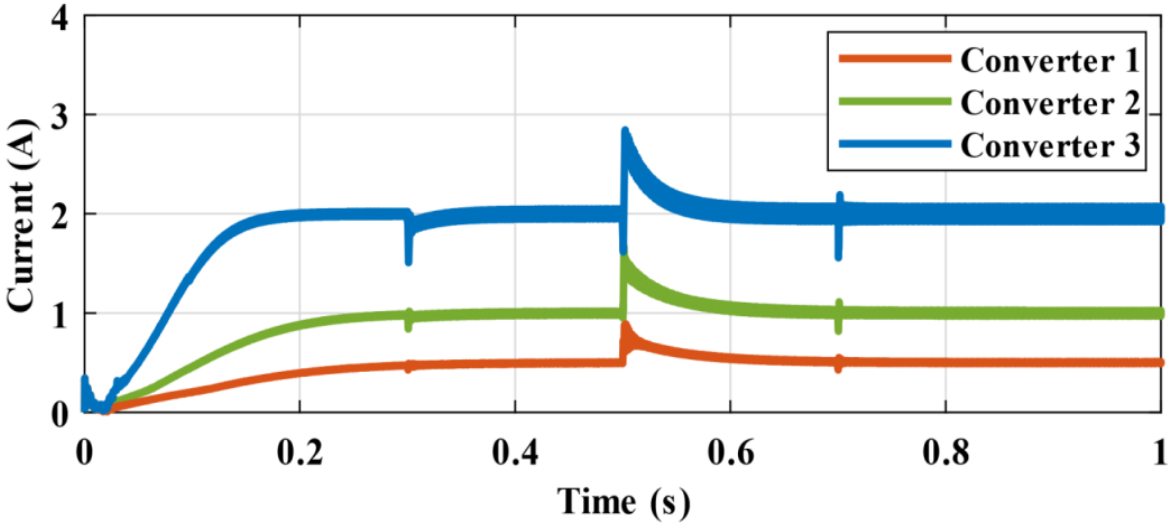

Fig. 21 Simulation results in Case Study 3: output current response for all power cells

Table 5 Control technique comparative analysis

Control algorithms	Characteristics	Advantages	Limitations
SMC [35]	• Robust control technique • Suitable for non-linear controls • Converges near the sliding surface	• Can perform under abrupt variations • Fast settling time • Simple structure	• Chattering effect due to irregular control law • Large overshoots
SSM [36]	• Continuous estimation of system states • Suitable for non-linear controls	• Quick transient response • Less overshoots	• Requires detailed model description • Complex implementation
MPC [30]	• Robust control technique • Suitable for non-linear controls • Predicts future values	• Quick tracking due to estimation-based technique • Can perform under abrupt variations • Fast response	• High computational time • Requires detailed model description • Complex algorithm
FLC [37]	• Suitable for non-linear controls • Appropriate for systems with ambiguous boundary conditions • Uses a rule base	• Less overshoots • Responsive to large variations • Mathematical model is not required	• High computational time • Complex structure • High settling time
PI [38]	• Easier to implement • Better performance in linear systems • The complexity level is very low	• Flexible to integrate with several control algorithms • Quick transient response • Easy to-tune gains	• Cannot perform in abrupt variations • Steady-state error, higher settling time, and large overshoots • Cannot be tunned online
Proposed PSO-PI	• Easier to implement • Suitable for linear and non-linear controls • Requires less control variables • Optimized control parameters	• Self-tunning of parameters • Quick transient response • Can perform under abrupt variations • Less overshoots	• Requires memory to store iterations

Note: SMC - sliding mode control; SSM - state space modeling; MPC - model predictive control; FLC - fuzzy logic control; PI - proportional integral; PSO-PI - particle swarm optimization – proportional integral

6. Conclusion

The proposed system fulfills the current and future energy requirements of commercial and domestic consumers. The system has three power cells with an individual DC-DC converter and PSO-tunned PI control. To verify the self-balancing performance of the system, extensive analysis was conducted on the circuit modeling of the converter. Furthermore, to verify the system performance, the input and output conditions of the system vary in different case studies. The transient response in all case studies is less than 0.15 s, and the voltage ripple is less than 5%. The maximum overshoot

was in case study 2 after the first transitions for all power cells at 0.2 s; for power cell 1, it was 10.5 V; for power cell 2, it was 22.5 V; for power cell 3, it was 42 V. The maximum undershoot was in case 3 in the third transition for all power cells at 0.7 s; for power cell 1, it was 5.2 V; for power cell 2, it was 10.5 V; and for power cell 3, it was 18.5 V. However, the proposed system has a quick transient response, and all the power cells were stable in all case studies, indicating the optimum operation of the proposed system. The PSO-tunned PI control has an optimum performance under varying input and output conditions. The computational time is higher for PSO-tunned PI controls, but the performance of the proposed system is significantly better than conventional PI control. Finally, the disseminated idea, discussion, and valuable statistics on the DC power system performance will facilitate magnifying the RES implementation in commercial and domestic applications that will also be a road map to achieve decarbonization and sustainable development goals (SDGs).

The future energy generation and consumption trends are shifting from AC to DC voltage. Therefore, the proposed system has presented a DC voltage multi-output architecture of power cells to cater the future energy requirements. However, this architecture can improve by integrating it with different renewable sources. Furthermore, numerous metaheuristic control schemes can apply to renewable sources to improve the overall efficiency of the power system.

Acknowledgment

The PETRONAS University of Technology Foundation (YUTP) supported this research for the project titled “Development of A Power Electronics-Based Controller for Integrations of Variable Low-Speed Wind Turbines to Smart Grid “(015LC0-285 – Institute of Autonomous System – Center for System Engineering).

References

[1] SRINIVASAN M., and KWASINSKI A. Control analysis of parallel DC-DC converters in a DC microgrid with constant power loads. *International Journal of Electrical Power & Energy Systems*, 2020, 122: 106207. DOI: 10.1016/j.ijepes.2020.106207.

[2] BURMESTER D., RAYUDU R., SEAH W., and AKINYELE D. A review of nanogrid topologies and technologies. *Renewable and Sustainable Energy Reviews*, 2017, 67: 760-775. DOI: 10.1016/j.rser.2016.09.073.

[3] LIPU M.S.H., MIAH M.S., ANSARI S., MERAJ S.T., HASAN K., ELAVARASAN R.M., AL MAMUN, A. ZAINURI M.A.A.M., and HUSSAIN A. Power Electronics Converter Technology Integrated Energy Storage Management in Electric Vehicles: Emerging Trends, Analytical Assessment and Future Research Opportunities. *Electronics*, 2022, 11(4): 562.

[4] LIPU M.S.H., ANSARI S., MIAH M.S., HASAN K., MERAJ S.T., FAISAL M., JAMAL T., ALI S.H.M., HUSSAIN A., MUTTAQI K.M., and HANNAN M.A. A review of controllers and optimizations based scheduling operation for battery energy storage system towards decarbonization in microgrid: Challenges and future directions. *Journal of Cleaner Production*, 2022, 360: 132188. DOI: 10.1016/j.jclepro.2022.132188.

[5] DHARMASENA S., OLOWU T.O., and SARWAT A.I. Bidirectional AC / DC Converter Topologies : A Review. In: *2019 SoutheastCon IEEE Conference*, 2019.

[6] SADABADI M.S. A Distributed Control Strategy for Parallel DC-DC Converters. *IEEE Control Systems Letters*, 2021, 5 (4): 1231-1236.

[7] MOAYEDI S., NASIRIAN V., LEWIS F.L., and DAVOUDI A. Team-Oriented Load Sharing in Parallel DC–DC Converters. *IEEE Transactions on Industry Applications*, 2015, 51(1): 479-490. DOI: 10.1109/TIA.2014.2336982

[8] MUMTAZ F., YAHAYA N.Z., MERAJ S.T., KANNAN R., SINGH B.S.M., and IBRAHIM O. Multi-Input Multi-Output DC-DC Converter Network for Hybrid Renewable Energy Applications. In: *2020 International Conference on Innovation and Intelligence for Informatics, Computing and Technologies*. 2021: 1-6. DOI: 10.1109/3ict51146.2020.9312026.

[9] MERAJ S.T., YAHAYA N.Z., HASAN K., LIPU M.S.H., ELAVARASAN R.M., HUSSAIN A., HANNAN M.A., and MUTTAQI K.M. A filter less improved control scheme for active/reactive energy management in fuel cell integrated grid system with harmonic reduction ability. *Applied Energy*, 2022, 312: 118784. DOI: 10.1016/j.apenergy.2022.118784.

[10] LU Y., KHAN Z.A., ALVAREZ-ALVARADO M.S., ZHANG Y., HUANG Z., and IMRAN M. A critical review of sustainable energy policies for the promotion of renewable energy sources. *Sustainability*, 12(12): 1-30, 2020. DOI: 10.3390/su12125078.

[11] SHER F., CURNICK O., and AZIZAN M.T. Sustainable conversion of renewable energy sources. *Sustainability*, 13(5): 1-4, 2021. DOI: 10.3390/su13052940.

[12] MOUSSA S., BEN GHORBAL M.J., and SLAMA-BELKHODJA I. Bus voltage level choice for standalone residential DC nanogrid. *Sustainable Cities and Society*, 2019, 46: 101431. DOI: 10.1016/j.scs.2019.101431.

[13] IEC. *LVDC: electricity for the 21st century. Technology Report*. The International Electrotechnical Commission, 2016: 1-58. https://www.iec.ch/basecamp/lvdc-electricity-21st-century

[14] KUMMARA V.G.R., ZEB K., MUTHUSAMY A., KRISHNA T.N.V., PRABHUDEVA KUMAR S.V.S.V., KIM D.-H., KIM M.-S., CHO H.-G., and KIM H.-J. A comprehensive review of DC-DC converter topologies and modulation strategies with recent advances in solar photovoltaic systems. *Electronics*, 2020, 9(1): 31. https://doi.org/10.3390/electronics9010031

[15] HOSSAIN M.Z., RAHIM N.A., and SELVARAJ J. Recent progress and development on power DC-DC converter topology, control, design and applications: A review. *Renewable and Sustainable Energy Reviews*, 2018, 81: 205-230. DOI: 10.1016/j.rser.2017.07.017.

[16] KOLLI, A. GAILLARD A., DE BERNARDINIS A., BETHOUX O., HISSEL D., and KHATIR Z. A review on DC/DC converter architectures for power fuel cell applications. *Energy Conversion and Management*, 2015,

105: 716-730. DOI: 10.1016/j.enconman.2015.07.060.
[17] JEREMY L.J., OOI C.A., and TEH J. Non-isolated conventional DC-DC converter comparison for a photovoltaic system: A review. *Journal of Renewable and Sustainable Energy*, 2020, 12(1). DOI: 10.1063/1.5095811.
[18] DIVYA NAVAMANI J., VIJAYAKUMAR K., and JEGATHEESAN R. Non-isolated high gain DC-DC converter by quadratic boost converter and voltage multiplier cell. *Ain Shams Engineering Journal*, 2018, 9(4): 1397-1406. DOI: 10.1016/j.asej.2016.09.007.
[19] HOSSAIN M.Z., RAHIM N.A., and SELVARAJ J. Recent progress and development on power DC-DC converter topology, control, design and applications: A review. *Renewable and Sustainable Energy Reviews*, 2018, 81: 205-230. DOI: 10.1016/j.rser.2017.07.017.
[20] HAO Y., LI, H. LI K., FANG C., and DING X. Single-switch boost converter with extremely high step-up voltage gain. *Journal of Power Electronics*, 2020, 20(6): 1375-1385. DOI: 10.1007/s43236-020-00155-y.
[21] CELIK M.A., GENC N., and UZMUS H. Experimental verification of interleaved hybrid DC/DC boost converter. *Journal of Power Electronics*, 2022, 22(6). DOI: 10.1007/s43236-022-00471-5.
[22] OTHMAN M.H., MOKHLIS H., MUBIN M., AB AZIZ N.F., MOHAMAD H., AHMAD S., and MANSOR N.N. Genetic Algorithm-Optimized Adaptive Network Fuzzy Inference System-Based VSG Controller for Sustainable Operation of Distribution System. *Sustainability*, 2022, 14(17): 10798. https://doi.org/10.3390/su141710798
[23] ARUNKUMARI T., and INDRAGANDHI V. A fuzzy controlled high gain DC-DC converter for renewable power generation. *Journal of Intelligent & Fuzzy Systems*, 2019, 36(5): 4165-4176. DOI: 10.3233/JIFS-169975.
[24] RANI P.H., NAVASREE S., GEORGE S., and ASHOK S. Fuzzy logic supervisory controller for multi-input non-isolated DC to DC converter connected to DC grid. *International Journal of Electrical Power & Energy Systems*, 2019, 112: 49-60. DOI: 10.1016/j.ijepes.2019.04.018.
[25] EGHTEDARPOUR N. A synergetic control architecture for the integration of photovoltaic generation and battery energy storage in DC microgrids. *Sustainable Energy, Grids and Networks*, 2019, 20: 100250. DOI: 10.1016/j.segan.2019.100250.
[26] ANDRES-MARTINEZ O., FLORES-TLACUAHUAC A., RUIZ-MARTINEZ O.F., and MAYO-MALDONADO J.C. Nonlinear Model Predictive Stabilization of DC-DC Boost Converters with Constant Power Loads. *IEEE Journal of Emerging and Selected Topics in Power Electronics*, 2021, 9(1): 822-830. DOI: 10.1109/jestpe.2020.2964674.
[27] BARTOLUCCI L., CORDINER S., MULONE V., and SANTARELLI M. Short-therm forecasting method to improve the performance of a model predictive control strategy for a residential hybrid renewable energy system. *Energy*, 2019, 172: 997-1004. DOI: 10.1016/j.energy.2019.01.104.
[28] HONG P., LI, J. XU L., OUYANG M., and FANG C. Modeling and simulation of parallel DC/DC converters for online AC impedance estimation of PEM fuel cell stack. *International Journal of Hydrogen Energy*, 2016, 41(4): 3004-3014. DOI: 10.1016/j.ijhydene.2015.11.129.
[29] WANG H., HAN M., HAN R., GUERRERO J.M., and VASQUEZ J.C. A decentralized current-sharing controller endows fast transient response to parallel DC-DC converters. *IEEE Transactions on Power Electronics*, 2018, 33(5): 4362-4372. DOI: 10.1109/TPEL.2017.2714342.
[30] AN F., SONG W., YU B., and YANG K. Model predictive control with power self-balancing of the output parallel DAB DC-DC converters in power electronic traction transformer. *IEEE Journal of Emerging and Selected Topics in Power Electronics*, 2018, 6(4): 1806-1818. DOI: 10.1109/JESTPE.2018.2823364.
[31] WANG J., SONG X, and ABD EL-LATIF A.A. Single-Objective Particle Swarm Optimization-Based Chaotic Image Encryption Scheme. *Electronics*, 2022, 11(16): 2628. https://doi.org/10.3390/electronics1116262
[32] FERMEIRO J.B.L., POMBO J.A.N., CALADO M.R.A., and MARIANO S.J.P.S. A new controller for DC-DC converters based on particle swarm optimization. *Applied Soft Computing*, 2017, 52: 418-434. DOI: 10.1016/j.asoc.2016.10.025.
[33] GARCÍA-TRIVIÑO P., GIL-MENA A.J., LLORENS-IBORRA F., GARCÍA-VÁZQUEZ C.A., FERNÁNDEZ-RAMÍREZ L.M., and JURADO F. Power control based on particle swarm optimization of grid-connected inverter for hybrid renewable energy system. *Energy Conversion and Management*, 2015, 91: 83-92. DOI: 10.1016/j.enconman.2014.11.051.
[34] MERAJ S.T., YAHAYA N.Z., HASAN K., LIPU M.S.H., MASAOUD A., ALI S.H.M., HUSSAIN A., OTHMAN M.M., and MUMTAZ F. Three-phase six-level multilevel voltage source inverter: Modeling and experimental validation. *Micromachines (Basel)*, 2021, 12(9): 1133. DOI: 10.3390/mi12091133.
[35] KARAMI-MOLLAEE A. Observer Dynamic Sliding Mode Control of DC-DC Converter to Extract the Maximum Power of Photovoltaic System Using Dual Sliding Observer. *Electronics*, 2022, 11(16): 2506. https://doi.org/10.3390/electronics11162506
[36] AZER P., and EMADI A. Generalized State Space Average Model for Multi-Phase Interleaved Buck, Boost and Buck-Boost DC-DC Converters: Transient, Steady-State and Switching Dynamics. *IEEE Access*, 2020, 8: 77735-77745. DOI: 10.1109/access.2020.2987277.
[37] OUDDA M., and HAZZAB A. Photovoltaic system with SEPIC converter controlled by the fuzzy logic. *International Journal of Power Electronics and Drive Systems*, 2016, 7(4): 1283-1293. DOI: 10.11591/ijpeds.v7i4.pp1283-1293.
[38] KESHAVARZI M.D., and ALI M.H. A novel bidirectional dc-dc converter for dynamic performance enhancement of hybrid ac/dc microgrid. *Electronics*, 2020, 9(10): 1-20. DOI: 10.3390/electronics9101653.

参考文:

[1] SRINIVASAN M. 和 KWASINSKI A. 具有恆定功率負載的直流微電網中並聯 直流-直流 轉換器的控制分析。國際電力與能源系統雜誌，2020年，122：106207。DOI：10.1016/j.ijepes.2020.106207。
[2] BURMESTER D.、RAYUDU R.、SEAH W. 和 AKINYELE D. 納米網格拓撲和技術綜述。可再生和可持續能源評論，2017年，67：760-775。DOI：10.1016/j.rser.2016.09.073。
[3] LIPU M.S.H.、MIAH M.S.、ANSARI S.、MERAJ

S.T. 、 HASAN K. 、 ELAVARASAN R.M. 、 AL MAMUN、A. ZAINURI M.A.A.M. 和 HUSSAIN A. 電力電子轉換器技術 電動汽車中的集成儲能管理：新興趨勢，分析評估和未來的研究機會。電子學，2022，11(4): 562.

[4] LIPU M.S.H.、ANSARI S.、MIAH M.S.、HASAN K.、MERAJ S.T.、FAISAL M.、JAMAL T.、ALI S.H.M.、HUSSAIN A.、MUTTAQI K.M. 和 HANNAN M.A. 控制器回顧和基於優化的調度操作面向微電網脫碳的電池儲能係統：挑戰和未來方向。清潔生產雜誌，2022, 360: 132188. DOI: 10.1016/j.jclepro.2022.132188。

[5] DHARMASENA S.、OLOWU T.O. 和 SARWAT A.I. 雙向交流/直流轉換器拓撲結構：回顧。在：2019年東南會議電氣和電子工程師學會 會議，2019年。

[6] SADABADI M.S. 並聯 直流-直流 轉換器的分佈式控制策略。電氣和電子工程師學會 控制系統快報，2021，5 (4)：1231-1236。

[7] MOAYEDI S.、NASIRIAN V.、LEWIS F.L. 和 DAVOUDI A. 並聯 直流-直流 轉換器中面向團隊的負載共享。電氣和電子工程師學會 行業應用彙刊，2015年，51(1)：479-490。DOI: 10.1109/TIA.2014.2336982

[8] MUMTAZ F.、YAHAYA N.Z.、MERAJ S.T.、KANNAN R.、SINGH B.S.M. 和 IBRAHIM O。用於混合可再生能源應用的多輸入多輸出 直流-直流轉換器網絡。在：2020年信息學、計算和技術創新與智能國際會議。2021：1-6。DOI：10.1109/3ict51146.2020.9312026。

[9] MERAJ S.T.、YAHAYA N.Z.、HASAN K.、LIPU M.S.H.、ELAVARASAN R.M.、HUSSAIN A.、HANNAN M.A. 和 MUTTAQI K.M. 具有諧波抑制能力的燃料電池並網系統中有功/無功能量管理的無濾波器改進控制方案。應用能源，2022年，312：118784。DOI：10.1016/j.apenergy.2022.118784。

[10] LU Y.、KHAN Z.A.、ALVAREZ-ALVARADO M.S.、ZHANG Y.、HUANG Z. 和 IMRAN M. 對促進可再生能源的可持續能源政策的批判性回顧。可持續性，12(12)：1-30，2020。DOI：10.3390/su12125078。

[11] SHER F.、CURNICK O. 和 AZIZAN M.T. 可再生能源的可持續轉換。可持續性，13(5)：1-4，2021。DOI：10.3390/su13052940。

[12] MOUSSA S.、BEN GHORBAL M.J. 和 SLAMA-BELKHODJA I. 獨立住宅直流納米電網的總線電壓電平選擇。可持續城市與社會，2019, 46: 101431. DOI: 10.1016/j.scs.2019.101431.

[13] 國際電工委員會。低壓差分信號：21世紀的電力。技術報告。國際電工委員會，2016：1-58。https://www.iec.ch/basecamp/lvdc-electricity-21st-century

[14] KUMMARA V.G.R.、ZEB K.、MUTHUSAMY A.、KRISHNA T.N.V.、PRABHUDEVA KUMAR S.V.S.V.、KIM D.-H.、KIM M.-S.、CHO H.-G. 和 KIM H.-J. 對 直流-直流 轉換器拓撲結構和調製策略以及太陽能光伏系統最新進展的全面回顧。電子學，2020年，9(1)：31。https://doi.org/10.3390/electronics9010031

[15] HOSSAIN M.Z.、RAHIM N.A. 和 SELVARAJ J. 電源直流-直流 轉換器拓撲、控制、設計和應用的最新進展和發展：綜述。可再生和可持續能源評論，2018年，81：205-230。DOI：10.1016/j.rser.2017.07.017。

[16] KOLLI, A. GAILLARD A., DE BERNARDINIS A., BETHOUX O., HISSEL D. 和 KHATIR Z. 電力燃料電池應用的直流-直流轉換器架構綜述。能源轉換與管理，2015, 105: 716-730. DOI：10.1016/j.enconman.2015.07.060。

[17] JEREMY L.J.、OOI C.A. 和 TEH J. 光伏系統的非隔離式傳統 直流-直流轉換器比較：綜述。可再生和可持續能源雜誌，2020年，12(1)。DOI：10.1063/1.5095811。

[18] DIVYA NAVAMANI J.、VIJAYAKUMAR K. 和 JEGATHEESAN R. 採用二次升壓轉換器和電壓倍增器單元的非隔離式高增益 直流-直流 轉換器。艾恩沙姆斯工程雜誌，2018年，9(4)：1397-1406。DOI：10.1016/j.asej.2016.09.007。

[19] HOSSAIN M.Z.、RAHIM N.A. 和 SELVARAJ J. 電源直流-直流 轉換器拓撲、控制、設計和應用的最新進展和發展：綜述。可再生和可持續能源評論，2018年，81：205-230。DOI：10.1016/j.rser.2017.07.017。

[20] HAO Y.、LI、H. LI K.、FANG C. 和 DING X. 具有極高升壓電壓增益的單開關升壓轉換器。電力電子學報，2020, 20(6): 1375-1385. DOI：10.1007/s43236-020-00155-y。

[21] CELIK M.A.、GENC N. 和 UZMUS H. 交錯式混合直流/直流升壓轉換器的實驗驗證。電力電子學報，2022, 22(6). DOI：10.1007/s43236-022-00471-5。

[22] OTHMAN M.H.、MOKHLIS H.、MUBIN M.、AB AZIZ N.F.、MOHAMAD H.、AHMAD S. 和 MANSOR N.N. 基於遺傳算法優化的自適應網絡模糊推理系統的配電系統可持續運行的低壓開關櫃控制器。可持續性，2022年，14(17)：10798。https://doi.org/10.3390/su141710798

[23] ARUNKUMARI T. 和 INDRAGANDHI V. 用於可再生能源發電的模糊控制高增益直流-直流轉換器。智能與模糊系統學報，2019, 36(5): 4165-4176. DOI：10.3233/JIFS-169975。

[24] RANI P.H.、NAVASREE S.、GEORGE S. 和 ASHOK S. 連接到直流電網的多輸入非隔離直流到直流轉換器的模糊邏輯監控控制器。國際電力與能源系統雜誌，2019，112：49-60。DOI：10.1016/j.ijepes.2019.04.018。

[25] EGHTEDARPOUR N. 一種用於在直流微電網中集成光伏發電和電池儲能的協同控制架構。可持續能源、電網和網絡，2019年，20：100250。DOI：10.1016/j.segan.2019.100250。

[26] ANDRES-MARTINEZ O.、FLORES-TLACUAHUAC A.、RUIZ-MARTINEZ O.F. 和 MAYO-MALDONADO J.C. 具有恆定功率負載的直流-直流 升壓轉換器的非線性模型預測穩定性。電氣和電子工程師學會電力電子新興和精選主題雜誌，2021, 9(1): 822-830。DOI：10.1109/jestpe.2020.2964674。

[27] BARTOLUCCI L.、CORDINER S.、MULONE V. 和 SANTARELLI M. 提高住宅混合可再生能源系統模型預測控制策略性能的短期預測方法。能源，2019，172：997-1004。DOI：10.1016/j.energy.2019.01.104。

[28] HONG P.、LI、J. XU L.、OUYANG M. 和 FANG C. 並聯直流-直流轉換器的建模和仿真，用於质子交換膜燃料電池堆的在線交流阻抗估計。國際氫能學報，2016,

41(4): 3004-3014. DOI：10.1016/j.ijhydene.2015.11.129。
[29] WANG H.、HAN M.、HAN R.、GUERRERO J.M. 和 VASQUEZ J.C. 分散式均流控制器賦予並聯 直流-直流轉換器快速瞬態響應。電氣和電子工程師學會電力電子彙刊，2018 年，33(5)：4362-4372。DOI：10.1109/TPEL.2017.2714342。
[30] AN F.、SONG W.、YU B. 和 YANG K. 電力電子牽引變壓器中輸出並聯轻拍直流-直流 轉換器的功率自平衡模型預測控制。電氣和電子工程師學會電力電子新興和精選主題雜誌，2018，6(4)：1806-1818. DOI：10.1109/JESTPE.2018.2823364。
[31] WANG J., SONG X. 和 ABD EL-LATIF A.A. 基於單目標粒子群優化的混沌圖像加密方案。電子學，2022 年，11(16)：2628。https://doi.org/10.3390/electronics1116262
[32] FERMEIRO J.B.L.、POMBO J.A.N.、CALADO M.R.A. 和 MARIANO S.J.P.S. 一種基於粒子群優化的 直流-直流 轉換器的新型控制器。應用軟計算，2017，52：418-434. DOI：10.1016/j.asoc.2016.10.025。
[33] GARCÍA-TRIVIÑO P., GIL-MENA A.J., LLORENS-IBORRA F., GARCÍA-VÁZQUEZ C.A., FERNÁNDEZ-RAMÍREZ L.M. 和 JURADO F. 基於混合可再生能源並網逆變器粒子群優化的功率控制 系統。能源轉換與管理，2015, 91: 83-92. DOI：10.1016/j.enconman.2014.11.051。
[34] MERAJ S.T.、YAHAYA N.Z.、HASAN K.、LIPU M.S.H.、MASAOUD A.、ALI S.H.M.、HUSSAIN A.、OTHMAN M.M. 和 MUMTAZ F. 三相六級多級電壓源逆變器：建模和實驗驗證。微型機械（巴塞爾），2021年，12(9)：1133。DOI：10.3390/mi12091133。
[35] KARAMI-MOLLAEE A. 直流-直流 轉換器的觀察器動態滑動模式控制，使用雙滑動觀察器提取光伏系統的最大功率。電子學，2022 年，11(16)：2506。https://doi.org/10.3390/electronics11162506
[36] AZER P. 和 EMADI A. 多相交錯降壓、升壓和降壓-升壓直流-直流 轉換器的廣義狀態空間平均模型：瞬態、穩態和開關動力學。電氣和電子工程師學會 訪問，2020，8：77735-77745。DOI：10.1109/access.2020.2987277。
[37] OUDDA M. 和 HAZZAB A. 具有模糊邏輯控制的單端初級電感轉換器轉換器的光伏系統。國際電力電子與驅動系統雜誌，2016，7(4)：1283-1293. DOI：10.11591/ijpeds.v7i4.pp1283-1293。
[38] KESHAVARZI M.D. 和 ALI M.H. 一種新型雙向 直流-直流 轉換器，用於增強混合交流/直流微電網的動態性能。電子學，2020，9(10)：1-20. DOI：10.3390/electronics9101653。